Journal of Petroleum Science and Engineering 212 (2022) 110250

Contents lists available at ScienceDirect

Journal of Petroleum Science and Engineering

journal homepage: www.elsevier.com/locate/petrol

Pour point depressant efficacy as a function of paraffin chain-length

Muh Kurniawan [a,b], Jens Norrman [a], Kristofer Paso [a,*]

[a] Ugelstad Laboratory, Department of Chemical Engineering, Norwegian University of Science and Technology, NO-7491, Trondheim, Norway
[b] LEMIGAS, Research and Development Centre for Oil and Gas Technology, Jakarta, Indonesia

ARTICLE INFO

Keywords:
Single-component wax
pour point depressant
Wax appearance temperature
Gelation temperature

ABSTRACT

Pour point depressant (PPD) activity mechanisms include solubilization, morphology alteration, and steric/entropic repulsion. A wealth of complex intermolecular interactions governs PPD efficacies in real crude compositions. The current study utilizes single-component model waxes (n-$C_{24}H_{50}$, n-$C_{28}H_{58}$, n-$C_{32}H_{66}$ or n-$C_{36}H_{74}$) dissolved in dodecane to reveal chain-length dependent PPD efficacies. Wax appearance temperature depression, effected by PPD, diminishes as paraffin chain-length increases. Stronger London van der Waals attractions between longer wax components effectively diminish PPD solubilization activity. Controlled-temperature centrifugation reveals partitioning of PPD polymers and paraffin waxes between solid and liquid phases. PPD polymers typically contain a polydisperse molecular weight distribution. The highest molecular weight PPD polymers partition preferentially to solid phases, including PPD aggregates and PPD-modified wax crystals. The lowest molecular weight PPD polymers remain preferentially soluble in the liquid phase, binding only weakly to precipitated wax. The presence of precipitated wax counteracts the solubilization activity of PPD polymer. At high precipitated wax fractions, PPD shows no wax solubilization activity. As the precipitated wax fraction decreases, the wax solubilization activity of the PPD progressively increases. The wax solubilization activity of the PPD attains a maximum at the WAT. Finally, the results are consistent with a single optimal polymer molecular weight for PPD activity occurring at a single temperature. PPD polymers larger than the optimal MW undergo a coil-to-globule transition prior to wax crystallization, deactivating the polymer. Polymers smaller than the optimal molecular weight show weaker binding to wax crystals, consistent with a smaller Gibbs free energy of binding, and partition preferentially to the liquid phase. Modern PPD formulations should utilize polymers that are tailored according to molecular weight. Optimally tailored PPD polymers should be less polydisperse in nature than current PPD formulations.

1. Introduction

The presence of paraffin wax in produced petroleum fluids gives rise to several commonly encountered flow assurance problems. Paraffin waxes in petroleum fluid comprise linear, branched, and cyclic long-chain saturated aliphatic hydrocarbons. Commercial paraffin waxes contain alkanes with a number of carbon atoms, $n_c \geq 17$ (Paso, 2005). The solubility of paraffin components in petroleum fluids increases strongly with increasing temperature. Paraffin components typically exist in a dissolved state in high pressure, high temperature (HPHT) petroleum reservoirs. As petroleum fluid flows along the length of a production string, thermal losses to the surrounding environment may cause the fluid temperature to fall below the wax appearance temperature (WAT). Resultant precipitation of solid wax crystals in the produced fluid causes various production challenges. Production problems originating from paraffin wax include wax deposition during continuous flow, pipeline plugging attributed to gelling during flow shut-in, increased fluid viscosity(Kelland, 2014), and emulsion stabilization (Rodriguez-Fabia et al., 2019).

The WAT value denotes the highest temperature at which paraffin crystallization transpires in a given petroleum fluid, at a specified pressure condition. The WAT value approximates the thermodynamic solubility limit of the wax. The WAT is an essential parameter for consideration while assessing whether wax related problems will arise in a given petroleum production system (Huang and Z. SFogler, 2015). Commonly used techniques for detecting the onset of wax crystallization in petroleum fluids include visual inspection (Ashbaugh et al., 2002; Production Chemicals for, 2010), differential scanning calorimetry (DSC), cross-polarized microscopy (CPM) (Roenningsen et al., 1991), viscometry (Bhat and Mehrotra, 2004), Fourier-transform infrared

* Corresponding author.
E-mail address: kristofer.g.paso@ntnu.no (K. Paso).

https://doi.org/10.1016/j.petrol.2022.110250
Received 9 October 2021; Received in revised form 1 January 2022; Accepted 29 January 2022
Available online 1 February 2022

spectroscopy (FTIR) (Roehner and Hanson, 2001), nuclear magnetic resonance (NMR) (Zhao et al., 2015), and near infrared (NIR) scattering (Zhao et al., 2015). Comparative studies are inconclusive in establishing the most accurate WAT determination method (Ruwoldt et al., 2018). For completely transparent waxy petroleum fluids(Coutinho and Daridon, 2005), visual inspection provides a suitable WAT determination method because it allows an isothermal holding time to be implemented simultaneously on sample batches.

The equilibrium amount of solid wax precipitated from a given petroleum fluid as a function of temperature defines a wax precipitation curve (WPC). Measurement techniques commonly used to establish the WPC include FTIR(Roehner and Hanson, 2001), NMR (Baltzer Hansen et al., 1991), and DSC (Roehner and Hanson, 2001; Martos et al., 2008). The WPC of a given petroleum fluid can also be established via separation-based techniques, which physically separate the precipitated solid and supernatant liquid phases. Conceptual implementation of phase separation is simple, but is highly time-consuming. However, solid separation is the only procedure that affords solid wax recovery for further characterization, analysis, and testing. The standard method *UOP 46–86 Paraffin wax content of Petroleum oils and Asphalt* provides an industrial standard based on solvent extraction. Other separation techniques commonly utilized include filtration (Martos et al., 2008; Coto et al., 2008; Pauly et al., 1998) and centrifugation (Roehner and Hanson, 2001; Han et al., 2010; Burger et al., 1981). Occluded liquids are often present in solid precipitated wax. Therefore, corrective methods must be applied to account for the presence of occluded liquids and obtain accurate WPC curves via separation.

Risk abatement strategies for wax-related problems may be categorized as either preventive or remedial, and may be subcategorized into thermal, chemical, and mechanical implementation measures (Kelland, 2014). Wax inhibitors and pour point depressants (PPD) are widely used in the petroleum production industry for flow assurance purposes. Polymeric PPDs were pioneered by application of polymethacrylates as lubricant viscosity modifiers in the mid-1930s (Rudnick, 2009). Currently, various polymeric chemistries are used and primarily fall into the categories of copolymerized ethylene, comb polymers, and nano-hybrids (Yang et al., 2015). The influence of paraffin chain-length on PPD performance is well established. The common agreement is that when the alkyl chain length in PPDs molecules approaches an average paraffin chain length, the interactions between the PPDs and the paraffin are favorable (Yang et al., 2015; Florea et al., 1999; Feng et al., 2014).

Model fluids are often used in petroleum research investigations to reduce the heterocomponent complexity of real petroleum fluids, and thereby isolate observation of the investigated processes of interest. Specification a model waxy fluid typically involves selection of a specified paraffin wax distribution along with a representative organic solvent in order to emulate the essential components of waxy petroleum fluid(Paso et al., 2014), while eliminating experimental artefacts arising from the behavior of other components. Typical model waxy oils contain a distribution of paraffin components. The paraffin distribution complicates a thermodynamic understanding of polymer-wax interactions, which become overshadowed by thermodynamic phenomena stemming from multi-paraffin precipitation. Hence, in the current article, single-component paraffins are utilized in a model fluid to isolate interactions between polymers and single paraffins, to elucidate both the physical nature and consequences of polymer-wax interactions. The overall motivation for selecting a monodisperse model paraffin is to simplify the thermodynamics and delineate the influence of inhibitor on effective low temperature wax solubility (*i.e.* wax solid fraction) versus morphological alteration. The fact that the selected model wax system comprised of monodisperse wax in solvent retains the distinct free energy of adsorption difference between the 2 primary crystal planes (–CH_2– and –CH_3 dominated planes, respectively) allows the model system to retain several essential physical characteristics of real polydisperse wax systems while revealing new mechanistic inhibition knowledge that is otherwise effectively concealed by artefacts arising the chain-length polydispersity. Hence, the selected model system is fully applicable to investigate the functional activity role of inhibitors in waxy petroleum fluid systems. In addition, using a monodisperse model wax system, substantial experimental protocol benefits and substantial experimental analysis benefits are provided by the compositional simplicity. For instance, proper interpretation of DSC heat flows are facilitated and substantially improved by an absence of artefacts that otherwise arise from polydisperse chain lengths. Specifically, in a monodisperse system, the residual heat flow at low temperatures converge with the heat capacity baseline, allowing proper identification of the true heat capacity baseline. In contrast, in polydisperse wax systems, the presence of low molecular weight paraffin components precludes low-temperature convergence of the measured heat flow signal with the heat capacity baseline, preventing proper identification of the heat capacity baseline. An undefined heat capacity baseline precludes proper heat signal integration and precludes observation of paraffin-additive interactions within the auspices DSC heat flow signals. In general, concealment of paraffin-additive interaction signals by multi-paraffin crystallization artefacts constitutes a ubiquitous problem in waxy oil research. Concealment of paraffin-additive interactions by multi-paraffin crystallization arises in various experimental probing techniques and is compounded by the polydispersity of polymeric additives. The specific problem of multi-paraffin crystallization is circumvented by using single paraffin components. Hence, utilization of single paraffin components allows the research thrust to focus on the influence of polymer molecular weight and polydispersity.

In the current investigation, techniques used to investigate phase behavior of PPD polymer and single-component paraffin wax in dodecane are visual turbidity observation, gelation point determination, cross-polarized microscopy, temperature-controlled centrifugation, and HPLC analysis. Temperature-controlled centrifugation and HPLC analysis are well-suited for studying solid-liquid phase partitioning of PPD polymer due to a combined ability to separate the phases and probe the wax content, polymer content, and polymer molecular weight distribution in each recovered phase. Temperature-controlled centrifugation provides appropriate sample amounts for subsequent HPLC analysis. These techniques collectively meet the need for obtaining new knowledge concerning partitioning of PPD polymers into various solid and liquid phases, for various polymer chemistries, molecular weight distributions, and wax chain-lengths.

2. Experimental section

2.1. Materials

Dodecane ($C_{12}H_{26}$ >99% purity from Sigma Aldrich) was selected as the solvent for the single wax-component model fluids. Four single component *n*-alkanes, with an even number of carbons, were selected to represent the paraffin wax: tetracosane (*n*-$C_{24}H_{50}$, hereafter denoted C24, 99% purity from Alfa Aesar), octacosane (*n*-$C_{28}H_{58}$, hereafter denoted C28, 98% purity from Aldrich), dotriacontane (*n*-$C_{32}H_{66}$, hereafter denoted C32, 97% purity from Aldrich), and hexatriacontane (*n*-$C_{36}H_{74}$, hereafter denoted C36, 98% purity from Aldrich). Four of five PPD polymers used in this work, PPD A, B, C, and D, are proprietary and were purified by evaporation, as they were originally supplied as dissolved in solvent. PPD E (EVA, 25% vinyl acetate, product number 437220) was purchased from Sigma Aldrich and used as received. Analytical grade toluene (Sigma Aldrich, 99.8%, anhydrous) was used as a rinsing solvent. Preparation of the model oil samples involved co-formulating wax, PPD, and dodecane.

2.2. Size-exclusion chromatography (SEC)

The molecular weight distribution of the PPD polymers was qualitatively determined via HPLC, utilizing a Shodex KF-803 packed bed

column and a Shimadzu SPD-20 A UV-detector with a measuring wavelength of 220 nm. THF was used as the bulk solvent at a flow rate of 1 mL/min, and molecular weight calibration was performed using five Shodex SM-105 polystyrene (PS) molecular weight standards, ranging from 1.22 to 124 kDa, providing a relationship between measured retention time and polymer molecular weight. The injection sample volume was 20 μL. For PPD concentration determination, a concentration series of known PPD dosages was used as standard solutions.

2.3. Visual turbidity observation

The model wax solution samples and PPD solution samples used in the current article were optically transparent at high temperature conditions. Therefore, visual turbidity observation was selected as an appropriate method to quantitatively measure the cloud point. For the case of model fluids containing only single-component *n*-paraffin and dodecane, measured cloud points correspond to the wax appearance temperature. For model fluids containing only PPD and dodecane, measured cloud points correspond to the polymer solubility threshold. For the case of model fluids containing single component *n*-paraffin, dodecane, and PPD, measured cloud points may correspond to the solubility threshold of *n*-paraffin or the polymer, depending on the component precipitation sequence. The visual turbidity measurement protocol was implemented as follows. A sample contained in a clear glass vial was heated to 65 °C in a water bath and was maintained at 65 °C for 60 min prior to cooling to approximately 5 °C above the predicted *CP*. Visual observation to examine for solution turbidity was conducted after equilibrating the sample for 15 min. Subsequently, cooling and solution turbidity examination was performed in a stepwise manner, at a prescribed temperature interval of 0.5 °C or smaller.

2.4. Gelation point determination

Rheological experiments were performed with an Anton Paar Physica MCR 301 Rheometer. The rheometer was fitted with 2° sandblasted cone and plate geometry of 4 cm diameter and gap of 170 μm. A sandblasted lower surface was used in conjunction with the sandblasted cone and plate geometry to reduce slippage. A Peltier plate in thermal communication with the fluid sample provided temperature control. The sample was loaded between the geometry and plate of the rheometer and allowed to equilibrate for 5 min at 60 °C (65 °C for the model fluid sample containing n-C_{36}). A constant oscillatory shear stress of 1.2 Pa was applied at a frequency of 1 Hz while implementing the thermal protocol to determine the gelation point. The data sampling interval was 15 s, corresponding to a data sampling temperature interval of 0.25 °C. A fast cooling rate of 20 °C min^{-1} was initially applied to reduce the temperature to a temperature of approximately 20 °C above the WAT. Subsequently, the cooling rate was controlled at 1 °C min^{-1} until a temperature of 4 °C was attained. The mechanical response of the fluid sample was characterized by G^*, which is defined as the ratio of the oscillatory stress amplitude to oscillatory strain amplitude. The gelation temperature of each model fluid sample was quantitatively ascribed to the location of the break in the G^* vs. temperature curve.

2.5. Cross-polarized microscopy (CPM)

CPM experiments were conducted with a Nikon Eclipse ME600 microscope fitted with a CoolSNAP-Pro camera from Media Cybernetics and cross-polarization filters. The combination of 10X/22 ocular lens and ELWD 10X/0.4 objective lens provided an overall magnification of 100 times. A CoolSnap-Pro monochrome digital camera from Media Cybernetics was utilized for image capturing. At 100 times magnification, a single frame captures an image with a dimension of 640 x 480 μm. Thermal control was provided by a PE 94 and LTS-120 E Peltier system from Linkam Scientific (UK). Samples were filled into rectangular glass capillaries with an inner cavity cross-section of 1 × 0.05 mm (width x height), sealed at the ends using 3 M Scotch cyanoacrylate glue, and fixed in place on a microscope slide. Air pockets were maintained between the sample and the glue to prevent contamination of the model fluid samples. The thermal protocol consisted of heating the model fluid to 60 °C for samples containing n-C_{24}, n-C_{28} or n-C_{32}, or alternatively to 70 °C for samples containing n-C_{36}, and subsequently maintaining the samples in an isothermal state for 15 min. Subsequently, model fluid samples were rapidly cooled to approximately 20 °C above WAT, and constant cooling was subsequently applied at a rate of 1 °C min^{-1}. Images were acquired after thermal equilibration at 25 °C or 4 °C for a minimum period of 30 min.

2.6. Wax equilibrium separation

Equilibrium separation of solid paraffin wax was performed by precipitation of a model paraffin wax solution at a specified temperature, according to the following protocol. Model wax solution samples were initially contained in glass vials. The model wax solutions in glass vials were preheated to 60 °C (or 70 °C for samples containing C36) in an oven for 1 h and subsequently homogenized to ensure complete solubilization of paraffin wax components. Subsequently, approximately 6–7 g of the thermally pretreated model wax solution was transferred to a 12 mL glass centrifugation tube. The centrifugation tube was sealed with a silicon stopper. The filled centrifugation tube was further thermally preconditioned for a period of 30 min by immersion in a water bath, but without further subsequent homogenization, to prevent silicon contamination of the model wax solution sample. After the 30-min thermal preconditioning stage, the water bath temperature was reduced to the equilibration temperature (4 °C, or alternatively 25 °C). The initial rate of cooling of the water bath fluid was observed to be approximately 2 °C per minute. For the model wax solution samples containing C32 or C36, the equilibration temperature for precipitation was selected to be 25 °C or 4 °C, while for the model wax solution samples containing C24 and C28, the equilibration temperature was set to 4 °C. The equilibration temperature was maintained for 4 h to allow sample equilibration. After thermal and phase equilibration, the sample was then transferred to a ThermoScientific Multifuge X3R centrifuge, preconditioned to the identical equilibrating temperature. Centrifugation was performed at 3000 rpm, providing an effective centrifugal force of 1960 (x g) for 90 min. The solid precipitated wax phase was deposited at the bottom of the tube, containing a substantial proportion of occluded liquid. The supernatant liquid phase was decanted into a glass vial. Using toluene as a rinsing solvent, the solid phase was transferred into a glass vial. Both separated phases were subsequently dried by solvent evaporation at 122 °C, assisted by continuously blowing nitrogen. The drying process effectively removed both the toluene and dodecane solvents. Deposits originating from both the liquid phase and the solid phase were finally weighed. Subsequently, SEC chromatography analysis was performed on the recovered solid material originating from the separated solid and liquid phases.

3. Results

3.1. PPD characteristics

Fig. 1 shows HPLC molecular weight distributions of the five PPD polymers, quantified by hydrodynamic volume-equivalent elution times calibrated to polystyrene. The quantitative separation capacity range of the Shodex KF-803 column is established as 10^3–10^5 Da equivalence in hydrodynamic volume to PS. Therefore, absolute molecular weight determination is valid only within this range. All PPDs show substantial UV signals outside of the requisite hydrodynamic volume range. Hence, quantitative determination of average PPD MW values is not valid. The presence of broad signal peaks for each sample confirms that the PPDs are polydisperse. PPD A and B, sharing a common nominal chemistry, appear to exhibit similar distributions in the high MW regime. PPD B

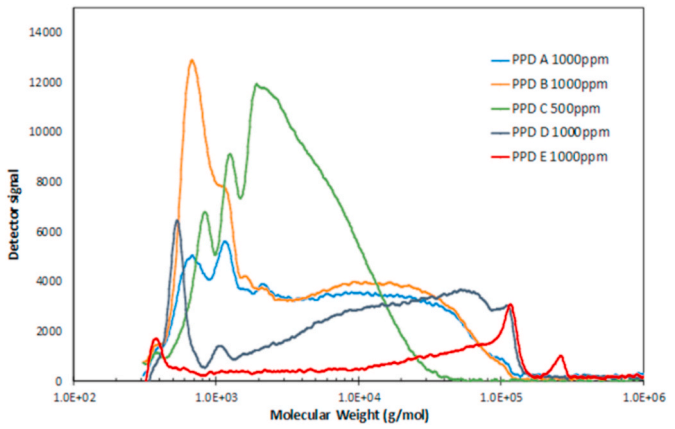

Fig. 1. Molecular weight distribution, defined in terms of hydrodynamic volume-equivalency to PS, as measured by size-exclusion chromatography, for all PPD samples.

also contains a substantial content of low MW oligomers with MW values of approximately 500–2000 Da equivalence to PS. PPD C has the lowest MW distribution, while PPD E has the highest MW distribution. PPD D and PPD E share a common EVA based chemistry. PPD E contains a considerable proportion of high MW components exceeding the column separation limit of 10^5 g/mol. For all PPDs, there is a considerable amount of substance with a molecular weight below the HPLC separability threshold of 10^3 g/mol equivalence to PS, comprising unreacted monomer and oligomers of low polymerization degree.

3.2. Cloud point

Measured cloud points of the model wax solutions and the PPD solutions in dodecane are shown in Table 2 and Table 3, respectively (see Table 1). Single component paraffins with longer carbon chains exhibit reduced solubility in dodecane and higher cloud points, due to stronger intermolecular interactions between the paraffin molecules. For the model solutions containing 5 wt% of single-component paraffin in dodecane, the measured cloud point increases by approximately 10 °C for each subsequent addition of 4 carbon atoms to the linear paraffin chain. Among the pour point depressants, PPD D and PPD E solutions have relatively high cloud points of 21.5 and 27 °C, respectively, in dodecane at a concentration of 1000 ppm. PPD A, B and C have cloud points below 10 °C in dodecane at a concentration of 1000 ppm. Based on SEC data, PPD D and E contain substantial proportions of high MW components that are most likely poorly soluble in dodecane. At the lower concentration of 300 ppm, all PPD solutions have cloud points that are 2–3 °C lower than the respective cloud points at 1000 ppm.

In comparing the measured cloud point values of the pristine model wax solutions and the PPD solutions in dodecane, it is observed that C32 and C36 have cloud point values higher than the cloud point values of all PPDs in dodecane at 300 ppm and 1000 ppm, confirming that paraffin nucleation and initial paraffin crystal growth ensues prior to bulk precipitation of the PPDs. Conversely, the cloud point values of PPD A, B, and C are lower than the cloud point values of all 5 wt% model wax solutions, indicating that PPDs A, B, and C remain completely soluble in the bulk fluid phase during initial wax nucleation and wax crystal growth processes.

Table 1
Characteristics of PPD.

PPD	Chemistry based on
PPD A	Polycarboxylate
PPD B	Polycarboxylate
PPD C	Polyacrylate, Ethylene vinyl acetate
PPD D	Polyacrylate, Ethylene vinyl acetate
PPD E	Ethylene vinyl acetate, 25% vinyl acetate content

Table 2
Cloud point of 5 wt% wax in dodecane.

Wax	Cloud point (°C)
C24	13.3 ± 0.3
C28	23.5 ± 0.3
C32	34.8 ± 0.5
C36	44.3 ± 0.3

Table 3
Cloud point of PPD in dodecane.

PPD	Cloud point (°C)	
	300 ppm	1000 ppm
A	5.5 ± 0.5	7.5 ± 0.5
B	8.0 ± 0.0	10.0 ± 0.0
C	6.0 ± 0.3	9.0 ± 1.0
D	18.0 ± 0.3	21.5 ± 0.5
E	24.5 ± 0.5	27.0 ± 0.0

The difference in cloud point of the pristine model wax solution and the doped model wax solution establishes the wax solubilization activity of the respective PPD polymer on a temperature basis. The cloud point (*CP*) depression is quantified as:

$$CP\ Depression = CP\ of\ untreated\ wax\ solution - CP\ of\ doped\ waxy\ solution \quad (1)$$

and the data is plotted in Fig. 2. For all doped model wax solutions, the measured *CP* depression is in the range of 0.5–3.5 °C. The observed wax solubilization activity, quantified as positive *CP* depression values, confirms that the five PPDs do not show activity as wax nucleators. For most model wax solutions, doping at 1000 ppm depresses the cloud point further than doping at 300 ppm.

For PPD A, B, and C, a significantly larger cloud point depression is observed for the model wax solution containing C24 than the other three paraffins. A dissimilar phenomenon is observed for PPD D and E, for which the C24 cloud point depression is smaller than the C28 cloud point depression. The cloud points of PPD D and E in dodecane are higher than the cloud point of C24 in dodecane. Therefore, a substantial portion of PPD D and E have already precipitated out of solution, via a coil-to-globule transition, when C24 crystallization ensues. Prior partial precipitation effectively reduces the soluble dosage amounts of PPD D and E. Precipitated polymers lack chain fluidity and are deactivated with respect to PPD performance. Hence, to achieve optimal PPD performance in cloud point depression, the PPD polymer should be in a soluble, coil-like state, with the requisite polymer chain fluidity, when wax crystallization ensues.

3.3. Gelation point

Oscillatory rheometry provides a measure of the gelation point of the model wax solutions. Traditionally, the gelation point is ascribed to the crossover point of the elastic storage (G') and viscous loss (G'') moduli. Accurate decomposition of the overall oscillatory torque amplitude required to establish the storage and loss moduli depends on an accurate phase angle determination by the instrument. Instrumental inertial artefacts and sample inertial artefacts influence the phase angle and are difficult to correct. A more robust method to establish the gelation temperature is to perform oscillatory rheology with a defined imposed oscillatory shear stress, and measure G^* as a function of temperature. The complex modulus G^* is not influenced by instrumental inertial artefacts or sample inertial artefacts appearing in the phase angle, provided that the total inertial moment of the instrument and geometry is well-established in the instrument calibration. The break in the G^* vs. temperature curve establishes a robust measure of the gelation

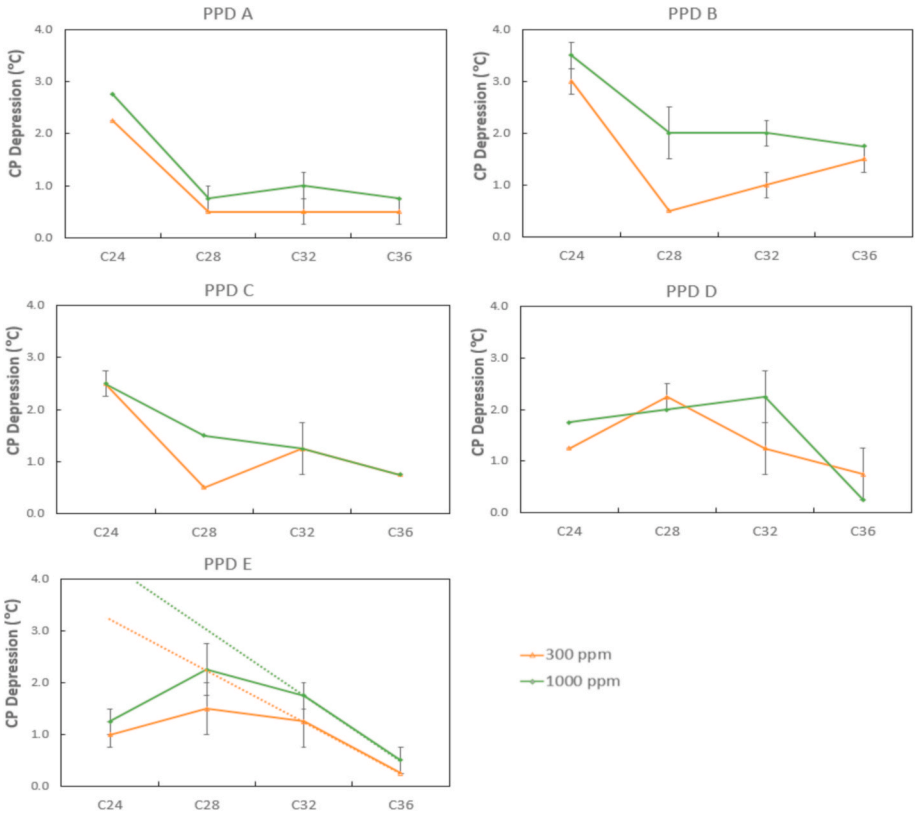

Fig. 2. CP depression of 5% wax in dodecane doped with PPDs at concentrations of 300 ppm and 1000 ppm. Visual turbidity observation experiments are conducted in duplicate. Dashed lines show idealized trends of CP depressions vs paraffin chain length.

temperature. Because the instrumental measurement of G^* is not influenced by instrumental inertial artefacts, the gelation temperature quantification by G^* provides a more robust estimation of the true gelation point in comparison to the often-unreliable G'/G'' crossover method. Specifically, the error in gelation temperature measured by the break in the G^* versus temperature curve does not contain any errors related to decomposition of the overall oscillatory torque signal to elastic and viscous rheological elements. The G^* method for establishing the gelation point is particularly well-suited to constant imposed oscillatory stress protocols, in which oscillatory fluid shearing imposed during the initial wax crystallization event effectively delays the gelation event by breaking incipient crystal-crystal bonds simultaneously as they form. The gelation event then occurs rapidly at a point in time where the effective gel strength surpasses the applied stress amplitude and crystal-crystal bond rupture ceases. The gelation event is accompanied by a rapid reduction in the oscillatory strain amplitude, which is manifested as a break in the G^* versus temperature curve. Because of the rapid gelation event associated with the defined oscillatory stress protocol, the G^* value immediately prior to the gelation event can be easily defined, and the G^* value immediately after the gelation event can be easily defined on a quantitative basis. The logarithmic average of the limiting G^* value immediately prior to the gelation event and the limiting G^* value immediately after the gelation event defines the gelation temperature, via interpolation.

The rapid gelation event, occurring under a small imposed oscillatory stress, yields satisfactory experimental reproducibility of the gelation temperature. Gel formation proceeds rapidly, as shown in Fig. 3, with the complex rheological modulus increasing from a magnitude of 10^{-2} to 10^{3} over a duration of ~1 min, corresponding to a temperature span of approximately 1 °C.

Table 4 shows measured gelation temperatures of the model wax solutions. Longer paraffin wax components yield higher gel temperatures, due primarily to solubility considerations. The gelation

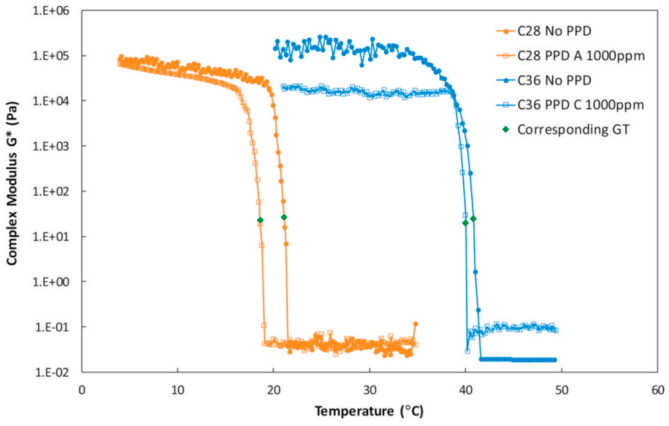

Fig. 3. G^* measurement during the gelation process.

Table 4
Gelation point of 5 wt% wax in dodecane.

Wax	Gelation point (°C)
C24	9.2 ± 0.2
C28	21.3 ± 0.2
C32	32.1 ± 0.3
C36	41.1 ± 0.4

temperature values are approximately 2–4 °C lower than corresponding cloud point temperatures measured by visual turbidity. The difference is due to a finite solid fraction requirement at gelation. Fig. 3 shows that PPD addition effectively delays the gelation event to lower temperature conditions. For model wax solutions containing C28, the measured G^*

moduli curve patterns are similar for doped and undoped solutions with PPD A. In other words, the entire G^* curve is shifted to lower temperatures by approximately 2.8 °C. The solubility shift of C28 by PPD A (as evidenced by the WAT reduction) accounts for a maximum of 0.5 °C of the overall gelation temperature shift, portending a morphological alteration and/or entropic/steric hindrance activity mechanism of PPD A. The effective activity mechanism of PPD A is not primarily solubility enhancement. In fact, the solubility enhancement activity of the PPD diminishes as the PPD leaves the liquid phase and binds to the solid precipitated paraffin wax.

For the model wax solution containing C36 in dodecane, addition of PPD C at 1000 ppm affects only a modest 1.3 °C reduction in gelation point. The solubility shift associated with the presence of 1000 ppm of PPD C may account for a maximum of 0.7 °C of the overall gelation point shift. Hence, morphological alteration and/or entropic/steric hindrance mechanisms account for at least ~0.6 °C of the overall gelation temperature reduction. However, the presence of 1000 ppm of inhibitor C effectively weakens the wax network structure and gel strength after the gelation event, as evidenced by a substantially reduced complex moduli value as the gel fully develops upon further cooling. As such, inhibitor C may be considered a more effective yield point depressant rather than a pour point depressant for the model wax solution containing 5 wt% C36.

The influence of PPDs on the gelation temperature can be quantified by the difference in gelation points of doped and un-doped samples. The gel point (*GP*) depression is calculated as:

$$GP\ Depression = GP\ of\ untreated\ wax\ solution - GP\ of\ doped\ wax\ solution \quad (2)$$

and the data is plotted in Fig. 4. In general, gelation point depression is more pronounced for model wax solutions containing shorter paraffin chains. However, this trend of greater efficacy for short paraffin chains is contingent upon the PPD polymer being in a completely soluble state upon incipient wax nucleation and crystallization. Therefore, PPDs D and E, which have high cloud points, show a dissimilar pattern with respect to gelation point efficacy as a function of paraffin carbon number. PPD E in dodecane has cloud points of 27 °C and 24.5 °C at concentrations of 1000 ppm and 300 ppm, respectively. Therefore, a substantial fraction of PPD E is unavailable for wax interactions when C24 crystallizes out of dodecane solution at a temperature of 13.3 °C, leading to a substantial reduction in the PPD efficacy in gelation point depression. A substantial fraction of the PPD polymer has precipitated out of solution by the time the temperature drops to the cloud point of C24, and C24 starts crystalizing out of solution. Similarly, PPD D has cloud points of 21.5 °C and 18 °C in dodecane at concentrations of 1000 ppm and 300 ppm, respectively. A similar reduction in the efficacy of PPD D is observed, but to a smaller extent than PPD E, due to the higher solubility of PPD D in dodecane in comparison to PPD E. The general trend among PPDs is that the gelation point depression is in the range of 0.5–3.2 °C, with a greater *GP* depression efficacy for short paraffin chains. In addition, doping with PPD at 1000 ppm typically depresses the gelation point further than doping with PPD at 300 ppm.

The rheometric gelation point and visual cloud point are compared by calculating the *CP-GP* difference as follows

$$CP - GP\ Difference = Visual\ Cloud\ Point - Rheometric\ Gelation\ Point \quad (3)$$

and the result is plotted in Fig. 5. Therefore, the value of *CP-GP* difference also reflects the solid fraction at the gelation event. Plotted data in Fig. 5 suggest that the different can be in the range of 1.4–4.8 °C.

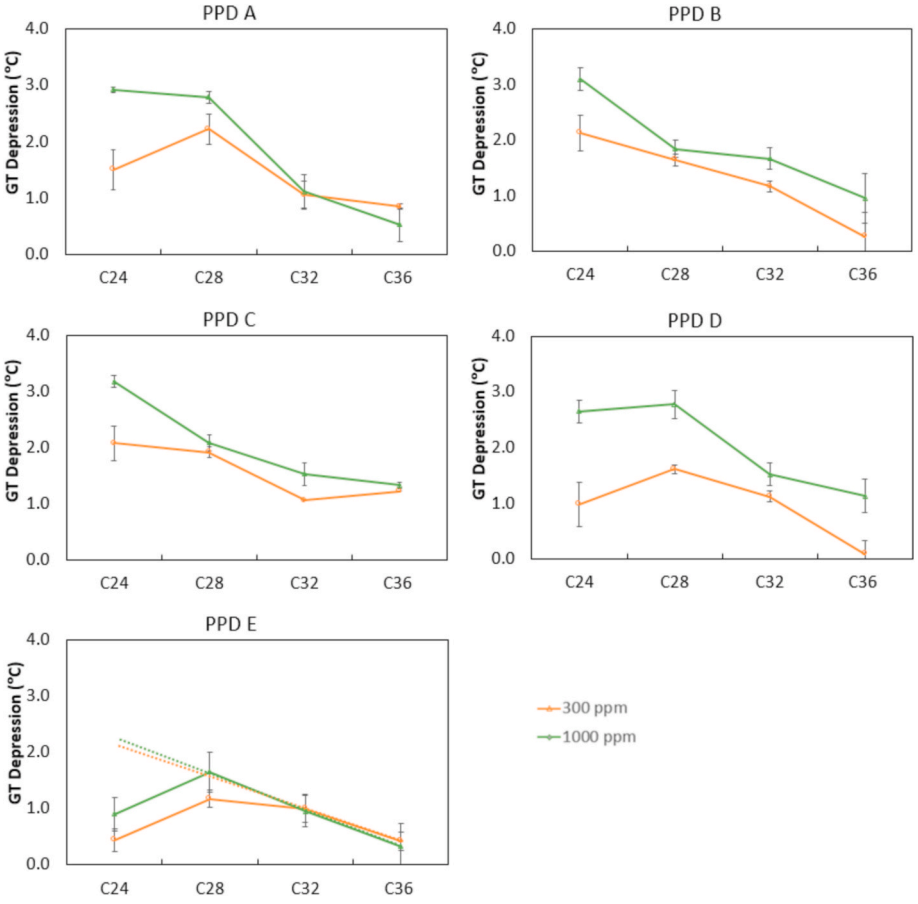

Fig. 4. Gelation point depression of 5% wax in dodecane doped by PPDs at concentrations of 300 and 1000 ppm. Rheometric experiments are conducted in duplicate. Dashed lines show idealized trends of GP depressions vs paraffin chain length.

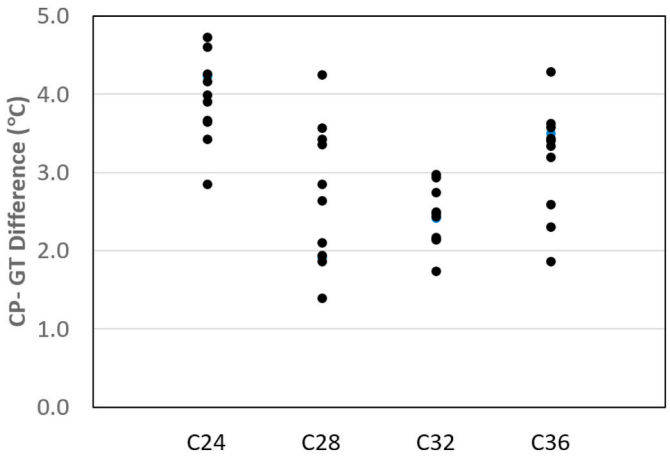

Fig. 5. Difference between Cloud Point and Gelation Point of all doped and undoped samples of 5% wax in dodecane. *CP-GP* Difference = Cloud point – Gelation Point.

3.4. Centrifugation, PPD separation

To study the solubility of PPD in solvent, centrifugation experiments are performed on PPD solutions in dodecane at 2 different temperatures: 4 °C and 25 °C. Controlled-temperature centrifugation separates the PPD solution into 2 fractions: (1) PPD precipitated as solid, and (2) PPD soluble in liquid phase.

The concentration of PPD in the liquid phase can be calculated as

$$PPD\ concentration\ in\ liquid\ phase\ (ppm) = \frac{Weight\ of\ PPD\ soluble\ in\ liquid\ phase}{Total\ weight\ of\ liquid\ fraction} \times 10^6 \quad (4)$$

Centrifugation separation results for all PPDs, at initial concentrations of 300 ppm and 1000 ppm, are presented in Table 5. Upon separation at 25 °C, PPD E at 300 ppm and 1000 ppm are shown to have concentrations of PPD in liquid phase of respectively around 183 ppm and 580 ppm, the least among all PPDs, which corroborates the high cloud point of PPD E in dodecane of 27 °C. Hence, a portion of the PPD E has precipitated out as solid material, which is corroborated by a substantial amount of PPD E observable as solid material after centrifugation at 25 °C. PPD D at 1000 ppm has a cloud point 21.5 °C, and the PPD D concentration that remains soluble in dodecane at 25 °C is 880 ppm. A trace amount of solid PPD D is observable at the bottom of the glass centrifuge tube after centrifugation at 25 °C. The concentration of PPD in liquid phase of PPD A, B, and C at 25 °C are all close to the initial concentration of the parent PPD. After centrifugation at 25 °C, precipitation is not observed from PPD A, B, and C, but the final recovery is not 100% because a certain amount of PPD may adsorb to the centrifuge tube wall during the separation process. At the lower temperature of 4 °C, all PPDs undergo substantial precipitation as the centrifugation temperature is below the respective PPD cloud points. PPD E exhibits the lowest concentration of PPD in liquid phase at 4 °C, consistent with the high cloud point.

Table 5
PPD concentration in liquid phase after separation at 4 and 25 °C, calculated by dividing the polymer recovered from the liquid phase by the liquid phase volume. Initial concentration of PPD, prior to separation, is 300 and 1000 ppm in dodecane.

PPD	PPD Concentration (ppm)			
	at 4 °C		at 25 °C	
	300 ppm	1000 ppm	300 ppm	1000 ppm
A	75	290	279	990
B	135	500	294	930
C	159	530	285	920
D	81	240	255	880
E	45	170	183	580

HPLC-SEC analysis is performed on the individual phase separated PPD fractions that have been diluted in THF. After HPLC analysis, the obtained HPLC signals are renormalized to reflect the PPD composition contained in the entire centrifugation sample volume.

Fig. 6 shows HPLC chromatograms of the original PPD A as well as its separated solid and liquid phase fractions, separated at 4 °C, and subsequently renormalized with respect to the initial overall centrifugation mass. It is evident that the solid phase fraction contains primarily high molecular weight components, while low molecular weight components preferentially partition to the liquid phase. This partitioning pattern is evident for all PPD types. High MW components have reduced solubility in the solvent and precipitate out at higher temperatures.

An attempt is made to utilize HPLC data to establish the concentration of PPD in liquid phase by area integration under the HPLC signal peak. For this purpose, the chromatogram is renormalized with respect to the weight of liquid phase recovered from centrifugation. The procedure for determining the HPLC-based PPD concentration involves proportioning of integrated signal area of liquid phase with respect to integrated signal area of parent PPD at initial concentration.

$$HPLC-based\ PPD\ concentration\ in\ liquid\ phase = \frac{Signal\ area\ of\ liquid\ phase\ PPD}{Signal\ areas\ of\ parent\ PPD} \times Initial\ concentration\ of\ parent\ PPD \quad (5)$$

Table 6 shows the HPLC-based concentrations of the liquid phase PPDs after separation by centrifugation at 4 °C and 25 °C. Theoretically,

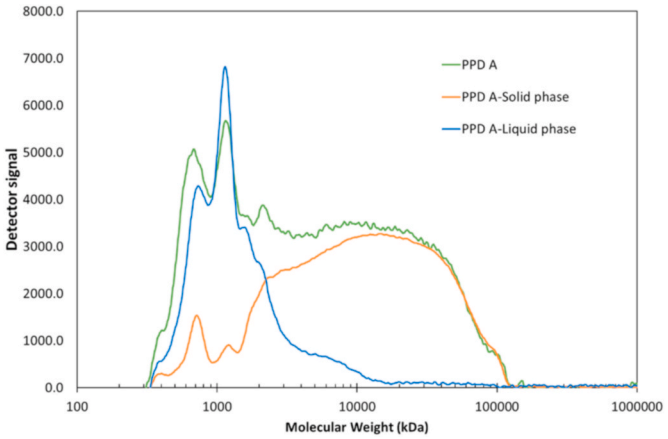

Fig. 6. HPLC-SEC chromatogram showing the molecular weight distribution of PPD A, PPD A in solid phase fraction, and PPD A in liquid phase fraction. The initial PPD concentration was 1000 ppm, and the separation was performed by centrifugation at 4 °C.

Table 6
Signal area proportions of liquid phase PPD after separation at 4 °C and 25 °C. Initial concentration of PPD before separation is 300 and 1000 ppm in dodecane.

PPD	at 4 °C		at 25 °C	
	300 ppm	1000 ppm	300 ppm	1000 ppm
A	169	443	307	1031
B	164	501	302	991
C	148	405	298	1003
D	89	195	264	890
E	86	291	153	624

this procedure would be applicable for absolute determination of PPD weight from wax-PPD mixtures. However, the HPLC-based PPD concentration in liquid phase is not consistent with the PPD concentration in liquid phase obtained by mass balance calculation as presented in Table 5. The liquid fraction does not have the same composition with the parent PPD. As a result, the UV detector response is not independent of MW. In the specific case of PPD A, lower MW fractions have a stronger UV absorbance signal response than the higher MW components. In the specific case of PPD E, lower MW fractions have a weaker UV absorbance signal response than the higher MW components.

Centrifugation is also performed on the 5 wt% wax solutions wax doped with PPD, providing separated liquid and solid phase fractions. Solid phase fractions contain large amount of wax with limited solubility in THF solvent. Highly diluted solutions in THF yield a low UV intensity signal from the HPLC detector. The separated liquid phase fractions contain substantially less wax and are re-dissolvable in THF at a relatively low degree of dilution. Therefore, HPLC-SEC analysis is performed on only the separated liquid phase fractions.

In the absence of PPD, HPLC chromatograms of wax exhibit a small peak at an approximate MW of 1000 g/mol equivalence to polystyrene. For HPLC determination of PPD concentration in samples containing wax, the integrated signal area attributed to the polymer is obtained by subtracting out the corresponding wax signal. Subsequently, the HPLC-based PPD concentration in liquid phase of doped wax solution can be determined by using eq. (5). HPLC-based PPD concentrations in the liquid phase of doped wax solutions are plotted in Fig. 7. (The 4 °C data for PPD E are omitted due to large data uncertainty attributed to low HPLC signal strength.)

For the above-mentioned reason of inconsistency between HPLC-based and mass balance based PPD concentrations, it must be note that the HPLC-based PPD concentration in liquid phase data in Fig. 7 are considered as relative comparisons among the samples, rather than absolute values.

After centrifugation, in the presence of solid C32 crystals or solid C36 crystals, the HPLC-based concentrations of PPD in liquid phase samples are substantially reduced in comparison to pristine PPD solutions, confirming that a certain amount of PPD has co-precipitated with solid wax and has been thereby sequestered from the liquid phase. Reductions in liquid phase PPD concentration are observed for PPD A, B and C, which have cloud points well below 25 °C, indicating that co-precipitation of wax and PPD polymer occurs despite the nominal self-solubility of the PPD in the liquid phase. The relative reduction in liquid phase PPD concentration in the presence of solid wax is more pronounced at 25 °C than at 4 °C, due to the higher liquid phase polymer concentration at the higher temperature condition. In addition, polymer chains available for co-crystallization at 4 °C are on average shorter, and have a weaker propensity to co-crystallize with solid paraffin wax. Fig. 8 provides a qualitative HPLC chromatogram comparison of the molecular weight

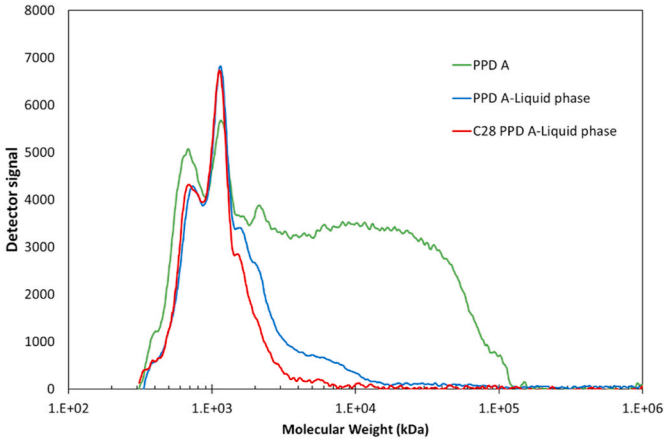

Fig. 8. HPLC-SEC chromatogram exhibiting molecular weight distribution of 1000 ppm PPD A in liquid phase, and liquid phase of 5 wt% C28 doped with 1000 ppm PPD A. The chromatogram for the liquid phase of 5 wt% C28 doped with PPD A chromatogram is obtained by subtracting the chromatogram of the liquid phase of undoped 5 wt% C28. Separation from dodecane solution is performed by centrifugation at 4 °C.

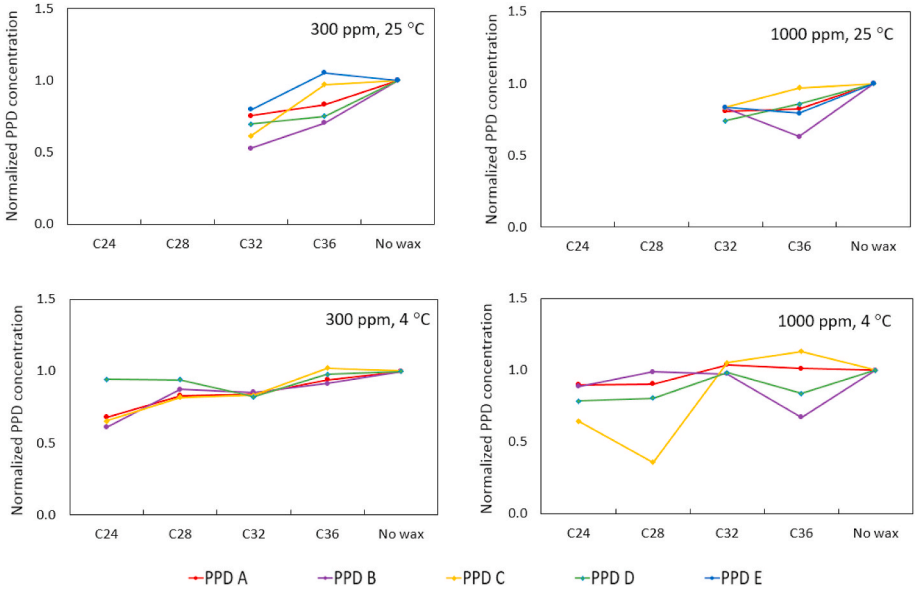

Fig. 7. Normalized liquid phase PPD concentration in the presence of solid wax.

distribution of PPD A in the liquid phase with and without the presence of solid C28 wax crystals. With the presence of solid C28 wax crystals, a substantial portion of moderate MW PPD A is removed from the liquid phase. Hence, the presence of precipitated solid C28 wax particles in the system induces additional co-precipitation of moderate MW PPD A, beyond the precipitated solid phase distribution of PPD A in the absence of solid C28 wax particles. Similar trends are also observed for the model oils containing PPD B, C, D, and E.

3.5. Centrifugation, wax separation

Equilibrium wax precipitation in dodecane under the influence of PPD is investigated by means of centrifugation. After undergoing a centrifugation at 1960×*g* for 90 min, wax model samples separate into two layers: a solid layer at the bottom of centrifugation tube and a top supernatant liquid phase. Separation of the solid and liquid phases is readily performed by decantation, and the weight of each phase is measured. The liquid phase contains dodecane solvent, the soluble portion of paraffin wax, as well as soluble PPD portion for the case of doped wax solution sample. Soluble PPD contributes a small proportion of the liquid phase composition. The absolute amount of PPD in the liquid phase cannot be determined by using the HPLC procedure. However, in the absence of solid wax, weighing the PPD recovered from the liquid phase, after dodecane evaporation, enables the determination of the PPD concentration in the liquid phase. This concentration, as presented in Table 5, provides a reasonable estimate for the PPD concentration in the liquid phase of the corresponding doped solutions.

In solid layer, three-dimensional network structure of wax crystals may occlude a substantial amount of liquid. Therefore, the solid layer comprises of solid precipitated wax, solid precipitated PPD, and occluded liquid. The occluded liquid is excluded from the solid phase, and assumed to have the same composition with the liquid phase, comprising of dodecane, soluble PPD, and soluble paraffin wax. Hence, the solid phase itself comprises of precipitated wax, precipitated PPD, and doesn't contain dodecane.

The overall weight fraction of precipitated wax in the solid phase, with respect to the initial wax contained in the sample, is calculated as

$$\textit{weight fraction of precipitated solid wax} = \frac{\textit{weight of wax in solid phase}}{\textit{weight of initial wax}} \quad (6)$$

Weight fraction of solid wax precipitated from undoped 5 wt% wax in dodecane at 4 °C and 25 °C is presented in Table 7. The weight fraction of precipitated wax reflects the insoluble portion of the wax in dodecane. At a given temperature, a longer paraffin chain exhibits lower solubility and therefore a larger fraction of the paraffin is precipitated out, compared to a shorter paraffin. At 4 °C, the precipitated fraction of C36 is close to unity, such that only a small proportion of the C36 remains soluble in dodecane. Wax solubility increases with increasing temperature; therefore, less paraffin wax is precipitated at 25 °C compared to 4 °C.

Weight fractions of paraffin wax precipitated out from doped model oils at 25 °C and 4 °C are presented in Fig. 9. An observable effect of PPD addition on the precipitated wax fraction is found for two cases. Specifically, an observable effect of PPD addition on the precipitated wax fraction is found on model oils containing C32 at 25 °C, which is 9.8 °C below the cloud point of undoped C32 in dodecane. Also, an observable effect of PPD C addition on the precipitated wax fraction is found for the model oil containing C24 at 4 °C, which is 9.3 °C below the cloud point of undoped C24 in dodecane. In these specific 2 cases, addition of PPDs unambiguously reduces the equilibrium weight fraction of solid precipitated paraffin wax. For the remaining separation cases (*i.e.*, C28 at 4 °C, C32 at 4 °C, C36 at 4 °C, and C36 at 25 °C), the temperature difference between the respective undoped cloud point and the equilibrium separation temperature is at least 19.3 °C. In these cases, the weight fraction of precipitated solid wax is high, as evidenced in Fig. 9. In these separation cases, characterized by a high weight fraction of precipitated solid wax, PPD doping into the wax solutions do not alter the wax precipitation to any appreciable extent. The wax solubilization activity of the PPD is completely diminished at a high solid wax fraction.

Table 7
Weight fraction of wax precipitated from 5 wt% wax solution in dodecane, separated by centrifugation at 4 °C and 25 °C.

Wax	weight fraction	
	4 °C	25 °C
C24	0.67 ± 0.025	–
C28	0.94 ± 0.010	–
C32	0.98 ± 0.005	0.83 ± 0.019
C36	0.99 ± 0.003	0.93 ± 0.010

3.6. Wax crystal morphology under cross-polarized microscope

Fig. 10 shows the two-dimensional wax crystal images taken under cross-polarized microscope observation at an overall magnification of 100X. The waxy oil sample is contained in capillary with a depth of 50 μm in order to limit the crystal growth in planar orientation. Fig. 10 (a) exhibits the crystal image of undoped 5 wt% C32 in dodecane at 25 °C demonstrating the typical morphology of pure n-alkane crystal, which is in thin and wide platelet shape. In Fig. 10 (b) is the crystal image of undoped 5 wt% C32 in dodecane at 4 °C, a continuation crystal growth from Fig. 10 (a), which exhibits the widening platelets as well as the rise of additional particles. Fig. 10 (c) shows the change in crystal morphology when 5 wt% C32 is doped with PPD A as much as 300 ppm. Upon addition of 1000 ppm PPD A as shown in Fig. 10 (d), the 5 wt% C32 crystals appear to be more disorder and hairy-like. In Fig. 10 (e) is a more developed image as the crystal in Fig. 10 (d) captured at 25 °C furtherly grow until 4 °C. Fig. 10 (f) and Fig. 10 (i) provide a crystal shape comparison of 5 wt% C36 in dodecane doped with 1000 ppm PPD E and PPD B respectively, captured at 4 °C. The series of Fig. 10 (g), (h), (j), and (i) demonstrate the comparison of the four waxes, respectively C24, C28, C32, and C36, when treated with 1000 ppm PPD B. The series of Fig. 10 (e), (j), (k), and (l) demonstrate the difference in crystal morphology when C32 treated with different types of PPDs, PPD A, PPD B, PPD C and PPD E respectively at the same concentration of 1000 ppm and temperature of 4 °C. Collectively, all PPDs show an ability to modify the crystal morphology, confirming the presence of physical interactions between the wax particles and the PPDs. Crystal morphology alteration to compact, coherent, and unconnected wax particle domains is known to yield optimal pour point depressant activity. In this respect, while all investigated PPDs modify the wax crystal morphology, none of the PPDs can completely counteract the tendency of single-component waxes to form thin platelets. Instead, high aspect ratios and/or inter-particle connectivity are evident for PPD-doped single-component wax crystals, corroborating the low magnitude of GP depression values shown in Fig. 4.

4. Discussion

Demonstrated performance activity of wax inhibitors is well documented for various end-use applications, including postponement of wax crystallization, gel point depression, pour point depression, gel-strength reduction, viscosity control, and deposition inhibition. However, the active inhibition mechanisms for waxy petroleum fluids remain a matter of debate(Yang et al., 2015; Oschmann, 1998), largely due to the wealth of complexity inherent to real petroleum fluid systems. Studies on polymer-wax interactions in model systems have previously been conducted by several authors (Yang et al., 2009, 2015; Wang et al., 2003; Chen et al., 2010; Soni and KiranbalaBharambe, 2008). In summary, polymeric wax inhibitors have five hypothesized modes of inhibition: (1) solubility enhancement, (2) crystal size alteration, (3) crystal morphology alteration, (4) imparting steric/entropic (Rudnick, 2009)

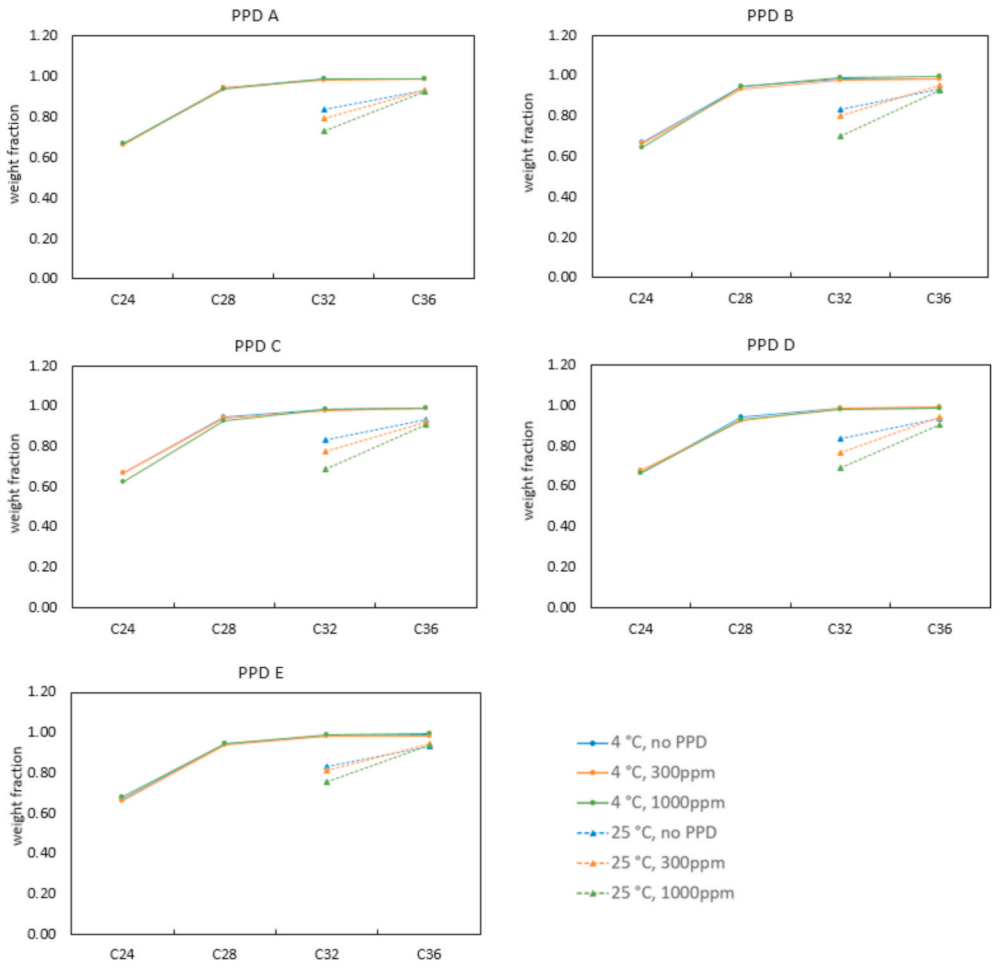

Fig. 9. Weight fraction of wax residing in the solid precipitated phase. Solid wax is separated by centrifugation from 5 wt% wax + PPDs in dodecane at 25 and 4 °C. The PPD concentrations are 300 and 1000 ppm.

hindrance, and (5) wettability alteration facilitating aqueous phase dispersion. Hypothesized sub-mechanisms of specific solid-phase polymer-wax interactions include co-crystallization and adsorption phenomena. However, co-crystallization and adsorption may not necessarily be mutually exclusive terms, as interfacial adsorption may readily occur in a structured, crystallographic manner for pendant aliphatic moieties on thin paraffin wax crystal side faces constituted by relatively high-interfacial-energy, orthorhombically structured $–CH_2–$ groups. As such, interfacial adsorption of comb-type or EVA-type polymers occurring without chain fluidity (for the pendant chains) may be considered a form of co-crystallization.

In the current work, monodisperse paraffin waxes are used, which provide fewer defects in the structure of the $–CH_3$ dominated crystal planes as compared to polydisperse waxes. The relatively defect-free $–CH_3$ surface provides a pronounced distinction between the free energy difference of adsorption of free paraffin chain from the bulk solution to the $–CH_2–$ dominated crystal plane and the $–CH_3$ dominated crystal plane, as compared with polydisperse waxes. As such, the model system constituted by monodisperse paraffin wax chain-lengths effectively highlights the real activity mechanism of the inhibitor interaction with respect to the high-interfacial-energy, orthorhombically structured $–CH_2$ dominated crystal plane. Hence, the selected model wax system in solvent is appropriate to investigate the physical nature of wax-inhibitor interactions at the high-interfacial-energy orthorhombically structured $–CH_2$ crystal planes.

For multi-paraffin wax crystals dominated by linear paraffin components, the thin $–CH_2–$ side planes grow quickly due to a high energetic driving force of adsorption for new wax molecules on the high-interfacial-energy crystal side faces and an absence of an adsorption free energy barrier for wax molecules. In contrast, paraffin chain addition on crystallographically unstructured (due to polydispersity in carbon chain length) $–CH_3$ dominated faces involves a spiral growth mechanism with a substantial associated free energy barrier that must be overcome in an interfacial nucleation and growth mechanism. Hence, the natural (unmodified) growth in crystal thickness occurs substantially slower than natural growth in crystal length and width, and high aspect ratios generally occur for unmodified wax crystals in organic solvent. Primary crystal aspect ratios are typically defined as the ratio of crystal length to crystal thickness or alternatively the ratio of the crystal width to crystal thickness. In terms of the total interfacial area of a wax crystal, high-aspect-ratio pristine wax crystals will usually have a high *areal* proportion of the crystal constituted by the crystallographically unstructured, low interfacial energy $–CH_3$ dominated top/bottom faces and a low *areal* proportion of the crystal constituted by orthorhombically structured, high-interfacial-energy, $–CH_2–$ side faces.

The low interfacial energy $–CH_3$ dominated faces are less crystallographically structured because of the polydispersity in paraffin chain length. For the $–CH_3$ dominated faces, the polydispersity in chain length is manifested throughout the crystal face area. The high interfacial energy, thin $–CH_2–$ side faces are highly orthorhombically structured, because the polydispersity in paraffin chain length is manifested only at the boundary edges between the high energy $–CH_2–$ side faces and the $–CH_3$ faces, and not throughout the crystal face area. This knowledge concerning the location of the crystal defects also provides a credible

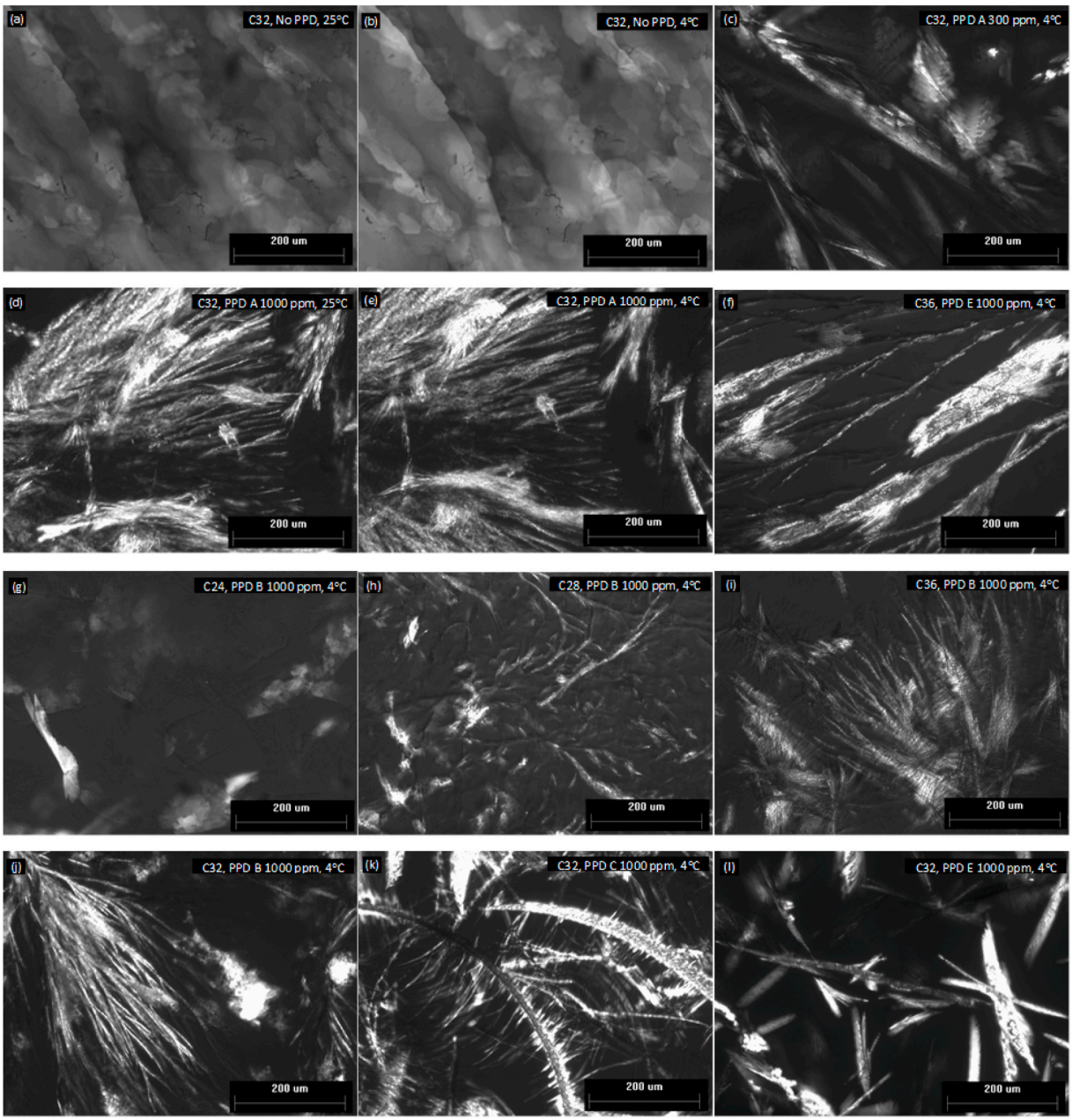

Fig. 10. Cross-polarized microscopy images of undoped or doped (1000 ppm PPD) 5 w.% wax in dodecane at stated temperatures **(a)** undoped C32 at 25 °C, **(b)** undoped C32 at 4 °C, **(c)** C32 with PPD A (300 ppm) at 4 °C, **(d)** C32 with PPD A at 25 °C, **(e)** C32 with PPD A at 4 °C, **(f)** C36 with PPD E at 4 °C, **(g)** C24 with PPD B at 4 °C, **(h)** C28 with PPD B at 4 °C, **(i)** C36 with PPD B at 4 °C, **(j)** C32 with PPD B at 4 °C, **(k)** C32 with PPD C at 4 °C, **(l)** C32 with PPD E at 4 °C.

rationale as to the reason why macro-crystalline wax responds more favorably to wax inhibitors than micro-crystalline wax. Micro-crystalline wax will not exhibit any relatively defect-free crystal side faces constituted by $–CH_2–$ groups, due to the ubiquitous presence of branched and cyclic paraffin components in the micro-crystalline wax. This knowledge also provides a credible rationale for the successful performance of wax inhibitors at concentrations as low as 100 ppm. The very low areal proportion of high interfacial energy $–CH_2–$ dominated surfaces in wax crystals requires only a very low concentration of interacting polymer to effectively disrupt the normal mode of crystallization and alter the resultant crystal morphology. In addition, the low energy $–CH_3$ dominated crystal faces exhibit low interaction with inhibitor polymers, reducing adsorptive depletion of the polymer on the low energy crystal faces. This very low areal proportion of high interfacial energy $–CH_2–$ dominated surfaces is successfully reproduced using single component waxes, retaining the essential interfacial feature of multi-component waxes in a simplified system enabling simplified solid-liquid thermodynamic equilibrium.

In comparison with the abundant areal proportion of the low-energy $–CH_3$ dominated faces, both co-crystallization and adsorption are most likely favored to occur on the high energy, orthorhombically structured $–CH_2–$ crystal edges, providing steric hindrance to additional paraffin crystallization on the altered $–CH_2–$ faces, as well as potential steric/entropic repulsion between modified wax crystals.

Limited current knowledge exists concerning the solid-phase interactions between paraffin wax crystals and inhibitor polymers. Paso et al. (2014) showed a distinct mechanistic difference between comb-type polymer interactions with wax crystals and copolymerized ethylene interactions with wax crystals, in a study performed with a polydisperse paraffin wax dissolved in a solvent. Co-polymerized

ethylene directly co-crystallizes with polydisperse paraffin wax crystals, substantially reducing the effective polydisperse wax solubility at low temperature conditions. In other words, the low-temperature solid fraction of precipitated polydisperse wax was substantially higher in the case of inhibition by copolymerized ethylene in comparison to the reference case without inhibition. Hence, for multi-paraffin waxes, copolymerized ethylene with an appropriate architecture may induce substantial additional wax precipitation by altering the thermodynamic character of the fluid (*i.e.* by addition of tethered aliphatic segments). In comparison, comb-type polymers exhibit only adsorption on wax crystal surfaces and do not exhibit co-crystallization phenomenon. In order to counteract the additional induced wax precipitation, it is hypothesized that co-polymerized ethylene likely also imparts substantial entropic/steric hindrance between wax crystals via inter-crystal repulsion arising from polymer chain segments extending into the bulk solution. The conventional morphological modulation mechanism alone may be unable to both (1) counteract the substantially increased solid fraction induced by copolymerized ethylene, and (2) provide a substantial inhibition activity performance. Hence, the inhibition activity mechanism of co-polymerized ethylene most likely involves entropic/steric repulsion in addition to modulation of crystal size and shape.

In the solid phase, the primary modes of interaction between wax molecules and pour point depressant polymers are known to be adsorption and co-crystallization. However, the functional activity of pour point depressant polymers is dependent upon architectural features such as pendant branch spacing for comb type polymers or vinyl acetate content for EVA type pour point depressant polymers. Industrial processes for manufacturing pour point depressant polymers typically result in broad molecular weight distributions for the base polymeric material, which is subsequently co-formulated along with suitable solvents and dispersants to provide a transportable formulation that can tolerate the low temperatures and small diameters of umbilical injection lines. The broad molecular weight distributions of the tailored PPD formulations are intended to allow co-crystallization or adsorption of pour point depressant polymers together with the polydisperse paraffin wax molecules over a broad range of temperatures in real waxy petroleum fluid systems. For instance, the co-crystallization process occurs concurrently with wax precipitation starting near the wax appearance temperature and continuing all the way down to the subsea environment temperature.

High molecular weight PPD polymers dispersed in the produced petroleum fluid tend to precipitate from the petroleum fluid at a high temperature condition, while lower molecular weight PPD polymers dispersed in the produced petroleum fluid will precipitate at lower temperature conditions. PPD polymers must be soluble in the liquid phase to co-crystallize with or adsorb on paraffin wax and modulate the paraffin wax crystal structure. Precipitated PPD polymers are effectively sequestered from the liquid phase and do not contribute to the inhibition activity. Hence, given the need to effectively function as pour point depressant polymers over the entire range of paraffin wax crystallization temperatures for a particular waxy petroleum fluid, the previous methodological assumption was that a tailored pour point depressant formulation should contain a broad range of polymer molecular weights that provide requisite co-crystallization or adsorption together with the respective range of wax components. The effective precipitation temperature for a given PPD polymer in a produced waxy petroleum fluid will also depend on the effective solvent strength provided by the light alkane components (and to a lesser extend the soluble heavier components) in the waxy petroleum fluid, which may vary considerably from fluid to fluid. Hence, there is a need to tailor and optimize the molecular weight distributions of PPD polymers for each specific produced petroleum fluid composition and corresponding range of operating temperatures. PPD polymers with molecular weights higher than the requisite range for wax co-crystallization will be sequestered from the liquid phase and thereby ineffective for the performance activity mechanism. PPD polymers with molecular weights lower than the requisite range for wax co-crystallization will preferentially partition to the liquid phase instead of co-crystallizing with or adsorbing onto the wax.

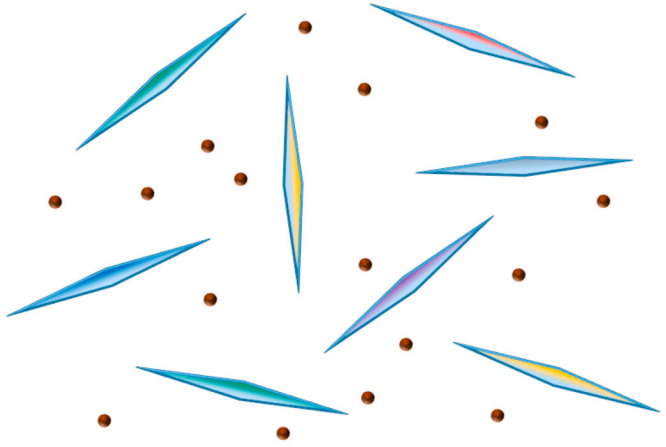

Fig. 11. Polymer dispersion and wax dispersion. Co-crystallized PPD polymer is present in the wax crystals.

At temperature conditions below the wax appearance temperature for waxy petroleum fluids, the presence of dispersed wax crystals influences the PPD polymer phase behavior. Specifically, additional binding of moderate MW PPD polymer to the wax crystal interface is observed when wax crystals are present. Fig. 11 shows a cartoon of precipitated PPD globules existing as dispersed particles alongside dispersed modified wax crystals. Fig. 11 is relevant for conditions in which the PPD cloud point is higher than the wax cloud point. At temperature conditions below the cloud points of both wax and PPD, the PPD polymer may physically exist in 1 liquid or 2 solid phases. Polymer partitioning behavior therefore involves a total of 3 phases, establishing a complex equilibrium balance. The PPD polymer precipitates prior to the onset of wax crystallization as relatively pure aggregates. Polymer aggregates comprise a relatively high MW fraction of the polymer and are effectively sequestered from the liquid phase and do not contribute to the performance activity of the PPD polymer.

The highest MW portion of PPD tends to precipitate out as polymer precipitates without interacting with solid wax. The lowest MW portion of the PPD will strongly partition to the liquid phase without interacting with solid wax. An optimum MW distribution of PPD polymer is required to establish optimum interaction between wax and polymer. The polymer molecular weight correlates strongly with the polymer solubility in the petroleum phase. In order to establish an optimum interaction with a particular wax component, the PPD polymers should be near the threshold of solubility at the wax crystallization temperature. Hence, the PPD cloud point cannot be too far below the wax crystallization temperature.

The above discussion represents polymer phase partitioning behavior occurring at a single specified temperature condition. Because inhibition and wax-polymer interactions occur over a broad range of temperatures associated with cooling a waxy petroleum fluid from the respective WAT to the seabed temperatures, an optimal molecular weight distribution may broaden substantially in comparison to the single optimum MW relevant for isothermal crystallization. However, beyond the optimal MW distribution broadening attributable to the broad temperature range of wax crystallization, the optimal distribution of polymer chain length does not require additional broadening with respect to paraffin wax polydispersity, provided that the tailored architectural features of the comb-type polymer or co-polymerized ethylene type polymer properly accommodate the given wax polydispersity.

5. Conclusions

Efficacy of five types of PPD are evaluated for simple model oils containing single component waxes in *n*-dodecane. Physical separation by centrifugation enables obtaining a solid phase and a liquid phase, and the composition of each phase can be determined accurately in a simple manner. In general, the amount of precipitated single-component paraffin wax is not influenced by PPD beneficiation. However, PPD polymer retains a moderate solubilizing effect for single-component paraffin waxes at temperatures in the proximity of the wax solubility threshold. We also note that the PPDs investigated in the current study do not exhibit the functional activity of wax nucleator-type PPDs, which are known to induce additional equilibrium precipitation of multi-component paraffin waxes.

Below the polymer cloud point, the polymer undergoes a coil-to-globule transition and progressively loses affinity to wax crystal interfaces. Solid polymer precipitates (*i.e.*, globules) comprise high MW polymer components, while lower MW components remain soluble in liquid phase. In the presence of precipitated solid wax, PPD concentration in the liquid phase is reduced in comparison to a base case without wax, confirming polymer binding with solid wax crystals.

PPD beneficiation to waxy model oils affects a substantial depression in the WAT as well as gelation temperature. PPD efficacy is substantially reduced when the polymer has undergone a coil-to-globule transition prior to the wax crystallization event. At such conditions, the solubilization efficacy of polymer is reduced because the precipitated polymers lose chain segment fluidity and do not contribute to liquid phase inhibition activity nor the interfacial binding activity mode. Low MW PPD, remaining soluble in the liquid phase after wax crystallization, also does not contribute substantially to inhibition activity.

The existence of a single optimal PPD molecular weight, relevant for isothermal crystallization conditions, arises from consideration of the polymer free energy of binding along with the inherent coil-to-globule transition of the polymer. Consider a very low MW fraction of a specific PPD polymer. Because of the very low MW, the binding free energy of the polymer to a wax crystal interface is very small, and the polymer will remain fully soluble in the liquid phase. As the MW of the polymer increases, the free energy of binding to the wax crystal interface increases, giving rise to stronger interfacial binding/adsorption/co-crystallization. As the MW further increases, polymer chain segments lose fluidity in the liquid phase because of the coil-to-globule transition, and the interfacial binding strength decreases with increasing MW. As such, the peak of the binding vs. MW curve represents a single optimal PPD molecular weight for isothermal wax crystallization. This single optimal polymer MW distribution will exhibit maximum solid phase wax interactions and without loss of polymer to solid phase polymer precipitates. For PPD activity occurring over a range of temperature conditions (for example during cooling), an optimal PPD MW distribution will broaden somewhat to accommodate the range of applicable thermodynamic conditions.

This new knowledge carries substantial implications for tailoring of commercial PPDs to real produced petroleum fluid compositions. Specifically, because it is primarily the high MW fraction of PPD that governs the PPD cloud point in a petroleum fluid, it is insufficient to simply match cloud points of wax and PPD in produced petroleum fluids, for proper PPD tailoring practices. The low MW and moderate MW PPD fractions must also be considered and tailored. The lowest MW fractions of the PPD polymer remain relatively inactive, and partition strongly to the liquid phase. In fact, at high solid wax fractions, liquid-phase PPD does not even show any solubilization activity. Instead, commercial PPDs should be formulated with substantially reduced polydispersity values and polymer MWs tailored to simultaneously eliminate PPD loss to pure solid PPD precipitation and maximize PPD interaction with solid wax crystals.

Finally, because PPD formulations themselves are known to gel and prevent flow within small-diameter intervention/umbilical lines, any inactive or weakly active polymer fraction should be removed from PPD formulations to promote PPD formulation flowability in small-diameter intervention/umbilical lines. Results from the current study show that current PPD formulations contain substantial inactive polymer fractions, including inactive low MW polymer fractions and inactive high MW polymer fractions. Concerted efforts should be made in the chemical vendor industry to develop MW tailoring practices for PPD polymers to specific fluids and specific temperature conditions, enabling substantially increased efficacy of future PPD formulations, while eliminating the risk of problems with PPD gelling in small diameter intervention/umbilical lines.

Author credit statement

All authors contributed equally to this manuscript.

Declaration of competing interest

The authors declare that they have no known competing financial interests or personal relationships that could have appeared to influence the work reported in this paper.

Acknowledgements

M.K. acknowledges the Ministry of Energy and Mineral Resources of the Republic of Indonesia for financial support during his Ph.D. studies. The authors acknowledge Michael Senra and Milind Deo for fruitful discussions.

Acronyms

CPM	cross-polarized microscopy
CP	Cloud Point
GP	Gelation Point
DSC	differential scanning calorimetry
EVA	ethylene vinyl-acetate copolymer
HPLC	high-performance liquid chromatography
PPD	pour point depressant
PS	polystyrene
SEC	size exclusion chromatography
THF	tetrahydrofuran
WAT	wax appearance temperature
WPC	wax precipitation curve

References

Ashbaugh, H.S., Radulescu, A., Prud'homme, R.K., Schwahn, D., Richter, D., Fetters, L.J., 2002. Interaction of paraffin wax gels with random crystalline/amorphous hydrocarbon copolymers. Macromolecules 35 (18), 7044–7053. https://doi.org/10.1021/ma0204047.

Baltzer Hansen, A., Larsen, E., Batsberg Pedersen, W., Nielsen, A.B., Roenningsen, H.P., 1991. Wax precipitation from North Sea crude oils. 3. Precipitation and dissolution of wax studied by differential scanning calorimetry. Energy Fuel. 5 (6), 914–923. https://doi.org/10.1021/ef00030a021.

Bhat, N.V., Mehrotra, A.K., 2004. Measurement and prediction of the phase behavior of wax-solvent mixtures: significance of the wax disappearance temperature. Ind. Eng. Chem. Res. 43 (13), 3451–3461. https://doi.org/10.1021/ie0400144.

Burger, E.D., Perkins, T.K., Striegler, J.H., 1981. Studies of wax deposition in the trans Alaska pipeline. SPE-8788-PA 33 (6), 1075–1086. https://doi.org/10.2118/8788-PA.

Chen, W., Zhao, Z., Yin, C., 2010. The interaction of waxes with pour point depressants. Fuel 89 (5), 1127–1132. https://doi.org/10.1016/j.fuel.2009.12.005.

Coto, B., Martos, C., Peña, J.L., Espada, J.J., Robustillo, M.D., 2008. A new method for the determination of wax precipitation from non-diluted crude oils by fractional precipitation. Fuel 87 (10), 2090–2094. https://doi.org/10.1016/j.fuel.2007.12.012.

Coutinho, J.A.P., Daridon, J.-L., 2005. The limitations of the cloud point measurement techniques and the influence of the oil composition on its detection. Petrol. Sci. Technol. 23 (9–10), 1113–1128. https://doi.org/10.1081/LFT-200035541.

Feng, L., Zhang, Z., Wang, F., Wang, T., Yang, S., 2014. Synthesis and evaluation of alkyl acrylate-vinyl acetate-maleic anhydride terpolymers as cold flow improvers for

diesel fuel. Fuel Process. Technol. 118, 42–48. https://doi.org/10.1016/j.fuproc.2013.08.005.
Florea, M., Catrinoiu, D., Luca, P., Balliu, S., 1999. The Influence of Chemical Composition on the Pour-Point Depressant Properties of Methacrylate Copolymers Used as Additives for Lubricating Oils, 12, pp. 31–44. https://doi.org/10.1002/ls.3010120103, 1.
Han, S., Huang, Z., Senra, M., Hoffmann, R., Fogler, H.S., 2010. Method to determine the wax solubility curve in crude oil from centrifugation and high temperature gas chromatography measurements. Energy Fuel. 24 (3), 1753–1761. https://doi.org/10.1021/ef901195w.
Huang, Z., Z S, Fogler, H.S., 2015. Wax Deposition: Experimental Characterizations, Theoretical Modeling, and Field Practices. CRC Press, Boca Raton. https://doi.org/10.1201/b18482.
Kelland, Malcolm A., 2014. Production Chemicals for the Oil and Gas Industry, 2 ed. CRC Press. https://doi.org/10.1201/b16648.
Martos, C., Coto, B., Espada, J.J., Robustillo, M.D., Gómez, S., Peña, J.L., 2008. Experimental determination and characterization of wax fractions precipitated as a function of temperature. Energy Fuel. 22 (2), 708–714. https://doi.org/10.1021/ef7003927.
Oschmann, Hans-Jörg, 1998. Das Kristallisationsverhalten von Paraffinen in Abhängigkeit von ihrer Zusammensetzung sowie seine Beeinflussung durch Paraffininhibitoren. PhD Thesis. Technische Universität Clausthal.
Paso, Kristofer G., 2005. Paraffin Gelation Kinetics. Ph.D. Dissertation. University of Michigan, USA.
Paso, K.G., Krückert, K.K., Oschmann, H.-J., Ali, H., Sjöblom, J., 2014. PPD architecture development via polymer–crystal interaction assessment. J. Petrol. Sci. Eng. 115, 38–49. https://doi.org/10.1016/j.petrol.2014.02.002.
Pauly, J., Dauphin, C., Daridon, J.L., 1998. Liquid–solid equilibria in a decane+multi-paraffins system. Fluid Phase Equil. 149 (1), 191–207. https://doi.org/10.1016/S0378-3812(98)00366-5.
Production chemicals for the oil and gas industry. Chromatography 72, 2010, 199. https://doi.org/10.1365/s10337-010-1557-2.
Rodriguez-Fabia, S., Lopez Fyllingsnes, R., Winter-Hjelm, N., Norrman, J., Paso, K.G., 2019. Influence of measuring geometry on rheomalaxis of macrocrystalline wax–oil gels: alteration of breakage mechanism from adhesive to cohesive. Energy Fuel. 33, 654–664. https://doi.org/10.1021/acs.energyfuels.8b02725.
Roehner, R.M., Hanson, F.V., 2001. Determination of wax precipitation temperature and amount of precipitated solid wax versus temperature for crude oils using FT-IR spectroscopy. Energy Fuel. 15 (3), 756–763. https://doi.org/10.1021/ef010016q.
Roenningsen, H.P., Bjoerndal, B., Baltzer Hansen, A., Batsberg Pedersen, W., 1991. Wax precipitation from North Sea crude oils 1. Crystallization and dissolution temperatures, and Newtonian and non-Newtonian flow properties. Energy Fuel. 5 (6), 895–908. https://doi.org/10.1021/ef00030a019.
Rudnick, L.R., 2009. Lubricant Additives: Chemistry and Applications. Taylor & Francis. https://doi.org/10.1201/9781420059656.
Ruwoldt, J., Kurniawan, M., Oschmann, H.J., 2018. Non-linear dependency of wax appearance temperature on cooling rate. J. Petrol. Sci. Eng. 165, 114–126. https://doi.org/10.1016/j.petrol.2018.02.011.
Soni, H.P., Kiranbala, Bharambe, D.P., 2008. Performance-based designing of wax crystal growth inhibitors. Energy Fuel. 22 (6), 3930–3938. https://doi.org/10.1021/ef8002763.
Wang, K.-S., Wu, C.-H., Creek, J.L., Shuler, P.J., Tang, Y., 2003. Evaluation of effects of selected wax inhibitors on wax appearance and disappearance temperatures. Petrol. Sci. Technol. 21 (3–4), 359–368. https://doi.org/10.1081/LFT-120018525.
Yang, F., Li, C., Lin, M., Li, Z., Yu, T., 2009. Depressive effect of polyacrylate (PA) pour point depressant on waxy crude oils. J. Petrochem. Univ. 22 (2), 20–25.
Yang, F., Zhao, Y., Sjöblom, J., Li, C., Paso, K.G., 2015. Polymeric wax inhibitors and pour point depressants for waxy crude oils: a critical review. J. Dispersion Sci. Technol. 36 (2), 213–225. https://doi.org/10.1080/01932691.2014.901917.
Zhao, Y., Paso, K., Norrman, J., Ali, H., Sørland, G., Sjöblom, J., 2015. Utilization of DSC, NIR, and NMR for wax appearance temperature and chemical additive performance characterization. J. Therm. Anal. Calorim. 120 (2), 1427–1433. https://doi.org/10.1007/s10973-015-4451-1.